Triplet Excited State Enhancement Induced by PDDA Polymer-Assembled Gold Nanoparticles

Chen Wang,[†] Xianwang Zhang,[‡] Kunhui Liu,*,[†] Xiaojuan Dai,[†] Chunfan Yang,[†] Shaoshi Guo,[†] and Hongmei Su*,[†]

[†]College of Chemistry, Beijing Normal University, Beijing 100875, P.R. China
[‡]Institute of Chemistry, Chinese Academy of Sciences, Beijing 100190, P.R. China

Ⓢ *Supporting Information*

ABSTRACT: Gold nanoparticles (AuNPs) have unique optical properties because of their characteristic localized surface plasmon resonances (LSPRs). Upon the excitation of LSPR, AuNPs can affect the adjacent organic molecules strongly in both the ground state and the excited state. Previously, only 2−3 fold of the plasmon enhancement effect on triplet state formation was displayed because of the random and uncontrollable formation of AuNP aggregates. Here, we utilize polymer PDDA to assemble AuNPs forming aggregates with strong plasmonic resonance. By means of transient UV−visible absorption spectroscopy, the triplet state of rose bengal enhanced by PDDA−AuNPs is directly monitored and the maximum enhancement is found to be ~10 fold. The large enhancement should be mainly resulted from the plasmon effect of AuNP aggregates. Additionally, it is found that the triplet state enhancement effect of PDDA-assembled AuNPs is sensitive to concentration of the polymer and the size of AuNPs. These findings shed light on the applications of AuNPs in triplet−triplet energy transfer, triplet exciton harvesting, and photodynamic therapy.
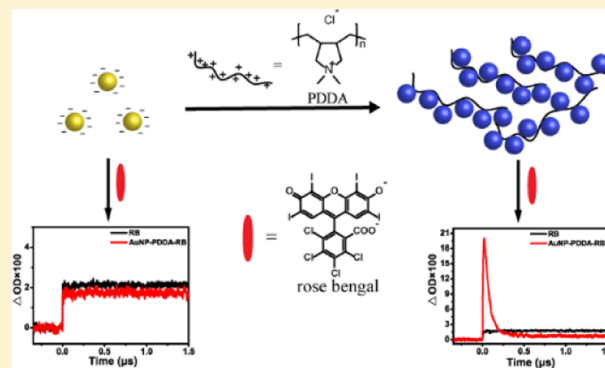
INTRODUCTION

Metal nanoparticles (NPs), such as silver and gold, can strongly interact with the adjacent organic molecules because of their unique localized surface plasmon resonances (LSPRs), which have received extensive attention in recent years.[1] These interactions include electron transfer from photo-excited molecules to metallic NPs[2,3] and energy transfer from metallic NPs to adjacent molecules.[4,5] Additionally, they can influence on the deactivation processes of excited molecules,[6] which make metallic NPs suitable for applications in surface-enhanced Raman scattering (SERS),[7−13] metal-enhanced fluorescence,[14−18] second-harmonic generation[19,20] two-photon excitation photoluminescence (TPPL),[21−24] and so forth. Nevertheless, the enhancement effect is not limited to the singlet excited state emission. Similar enhancement effects on triplet excited state formation should also be anticipated via intersystem crossing (ISC) from the excited singlet state, as reported for metal-enhanced phosphorescence (MEP).[25]

Normally, the triplet excited state of molecules can be detected by phosphorescence or transient absorption. Geddes et al. reported MEP using rose bengal (RB) at low temperature (77 K). Silver island films (SiFs) in close proximity to RB significantly enhanced phosphorescence emission intensity by fivefold, suggesting that surface plasmon coupled to triplet states can enhance phosphorescence yields.[25] Li et al. observed a 330 times enhanced phosphorescence from ³MLCT of

[Ru(bpy)₃]²⁺ by silver core silica shell-isolated NPs in the solid state.[26] Obviously, the experimental condition under very low temperature or under the solid phase are required to measure phosphorescence, which is not feasible for monitoring the triplet excited states of the sample in the liquid phase.

By using transient absorption spectroscopy, Scaiano et al. first reported the triplet state enhancement of methylene blue (³MB*) by a factor of ~2.2 upon addition of gold NPs (AuNPs).[27] Recently, we demonstrated that the enhancement effect on the triplet excited state resulted from the aggregation of AuNPs by comparing the circumstances of aggregated AuNPs and monodispersed AuNPs.[28] The triplet state enhancement effect was ascribed to the coupled electromagnetic fields of AuNPs, namely, hot spots, which resulted from AuNPs aggregation after addition of cationic dye molecules,[28] whereas the distribution of the dye in the unprotected AuNP aggregates was random and disordered. In this situation, the plasmonic field was not strong enough, and a smaller enhancement effect on the triplet state was displayed with only 2−3 times at initial formation time. Additionally, although the cationic organic compounds can strongly promote the aggregation by breaking of repulsive
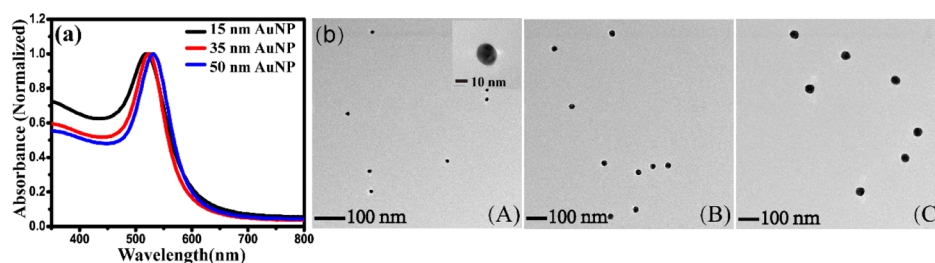
Figure 1. (a) UV−visible absorption spectra of citrate-stabilized AuNPs. Black line: 15 nm AuNPs, red line: 35 nm AuNPs, and blue line: 50 nm AuNPs. (b) TEM images of citrate-stabilized AuNPs of three sizes: (A) 15 nm AuNPs, (B) 35 nm AuNPs, and (C) 50 nm AuNPs.

interaction of the negative citrate-stabilized AuNPs due to charge neutralization, this type of aggregated metal NPs was not stable. As time goes on, the aggregated metal NPs all precipitated.

In order to regulate the formation of aggregates, many methods have been utilized, such as surfactants,[29,30] bifunctional organic molecules,[30−32] polyelectrolytes[7,21,22] and DNA double strands.[33] Polavarapu and Xu adopted water-soluble cationic conjugated polymer PFP to induce formation of chain-like AuNP aggregates,[7] by which a huge reproducible SERS enhancement factor of 8.4×10^9 was obtained. Another positively charged polymer poly(diallyldimethylammonium chloride), PDDA, has been used to assemble AuNPs as a colorimetric sensor in quantitative analysis of biomolecules such as proteins.[34,35] Xu et al. also utilized PDDA to induce AuNPs with different size to form chainlike Au aggregates, which achieved 25-fold enhancement on the TPPL.[22]

Intrigued by such strategies, herein, we use PDDA to assemble citrate-stabilized AuNPs forming dense aggregates. The zeta potential measurement indicates that PDDA−AuNPs assemblies are positively charged and have the ability to adsorb the anionic dye molecules RB. By means of time-resolved UV−visible absorption spectroscopy, the triplet state of RB is observed to be enhanced by a maximum of ~10-fold in the presence of PDDA−AuNPs. The higher enhancement on the triplet excited state might be mainly caused by the strong plasmon effect brought by the PDDA−AuNPs aggregates, in addition to the external heavy atom effect because of the close proximity between RB and Au particles. These results have prospect on the applications of AuNPs triplet−triplet annihilation up conversion,[36−38] triplet exciton harvesting,[4,39] and photodynamic therapy.[40,41]

■ EXPERIMENTAL SECTION

Materials. Tetrachloroauric acid ($HAuCl_4 \cdot 3H_2O$, ≥99.9%) was purchased from Sinopharm Chemical Reagent Beijing Corporation Ltd. Sodium citrate tribasic dihydrate (ACS Reagent, ≥99.0%) and PDDA solution (average M_w 400 000−500 000, 20 wt % in H_2O) were purchased from Sigma-Aldrich. RB was purchased from Alfa Aesar. All the reagents were used without further purification. Ultrapure water (18.2 MΩ cm, Milli-Q water, Millipore) was used in the chemical synthesis and aqueous solution preparation steps. All glassware was cleaned by aqua regia solution (HCl/HNO_3 = 3:1) and then rinsed by ultrapure water thoroughly.

Synthesis of AuNPs. The AuNP solution was prepared by the standard sodium citrate reduction method.[42,43] Briefly, 150 mL of tetrachloroauric acid solution was prepared in a 250 mL flask and brought with boiling and refluxing under vigorous stirring. Then, sodium citrate dihydrate solution was quickly

added into the flask. The solution was kept boiling and stirring for 20 min after it turned dark red in a few minutes. After that, the solution was cooled down to room temperature and stocked in the dark place. Larger-sized AuNPs were synthesized by the seed-mediated growth method as reported elsewhere with some modifications.[44] The Au seeds were prepared as mentioned above. The reaction temperature was cooled down to 70 °C. Then, 120 mL of AuNPs solution was extracted and 110 mL of H_2O was added. After that, 3.5 mL of 60 mM sodium citrate solution was added and 1 mL of 25 mM of a $HAuCl_4$ solution was sequentially injected after 2 min. The reaction was finished in 30 min. This process was repeated again. After that, the sample (55 mL) was extracted and diluted by using 51 mL of water and 2 mL of 60 mM sodium citrate. The process was repeated several times to obtain different-size AuNPs.

Transmission Electron Microscopy Measurement. The diameter of different-sized AuNPs was characterized by FEI Talos F200S transmission electron microscopy (TEM). The NP sample was prepared by dropping gold solution on the carbon-coated copper grids and then dried at room temperature.

UV−Vis Absorption Spectroscopy. The absorption spectra of RB, AuNPs, and their mixtures were measured by using the UV−vis spectrometer (model U-3900, Hitachi). The quartz cuvettes with 1 cm thickness were used in experimental detections. The concentration of RB was fixed at 5 μM. PDDA repeat units were fixed at 10 and 20 μM respectively. The SPR absorption intensity was fixed at 0.5 for different-sized AuNPs. Each mixture was shaken and equilibrated at room temperature for 1 min to ensure good mixing before the measurement.

Dynamic Light Scattering and Zeta Potential Measurements. To measure the hydrodynamic sizes and zeta potential of AuNPs, dynamic light scattering (DLS) and zeta potential measurements were conducted by using a Zetasizer Nano ZS (Malvern Instruments Ltd., UK) equipped with a 633 nm laser. All the measurements equilibrated with 120 s in 25 °C water. In each measurement, the number of runs and duration were set automatically.

Time-Resolved UV−Visible Absorption Spectroscopy. The nanosecond time-resolved laser flash photolysis was used to measure the decay kinetics of triplet RB and their transient UV−visible spectra which has been described elsewhere.[45] In brief, an LP980 spectrometer (Edinburgh Instruments, UK) is synchronized with a commercial Nd:YAG laser (Lab 170, Spectral Physics Inc.). Laser pulse (532 nm) (1 Hz, fwhm ≈ 7 ns, 20 mJ/pulse) was used to irradiate the sample solution in 1 cm thickness quartz cuvettes. A 150 W pulsed xenon lamp was used as the probe light. A photomultiplier (PMT) comprising a monochromator was used to collect the kinetic traces at certain
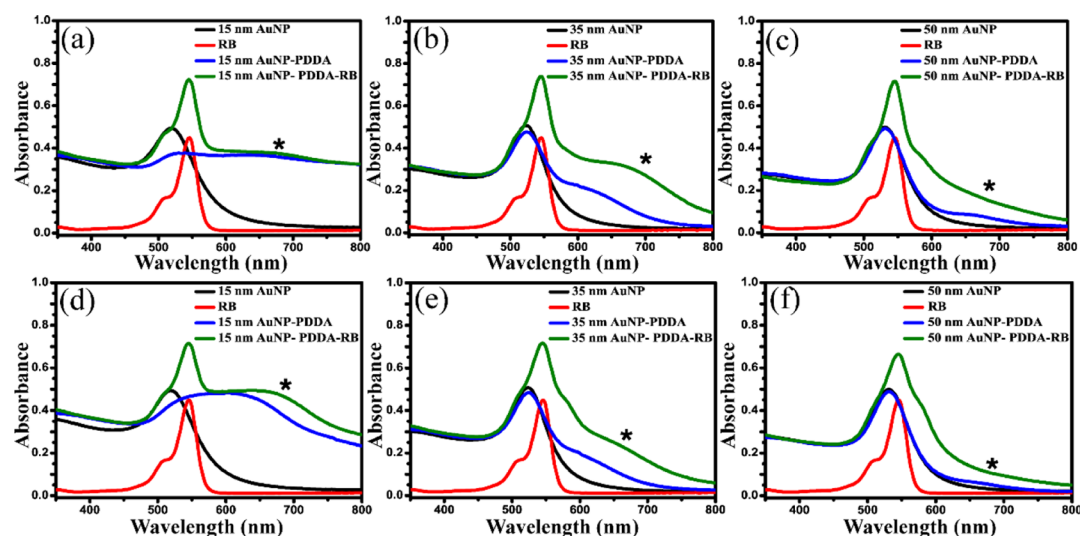
Figure 2. UV−visible absorption spectra of AuNPs. (a,d) 15 nm AuNPs; (b,e) 35 nm AuNPs; (c,f) 50 nm AuNPs. Black line: AuNPs; red line: RB; blue line: PDDA−AuNPs; and green line: RB with PDDA−AuNPs. The concentrations of repeat units PDDA were 10 μM for (a−c) and 20 μM for (d−f), respectively. The asterisk in the figure represents the plasmon band of the AuNPs aggregates.
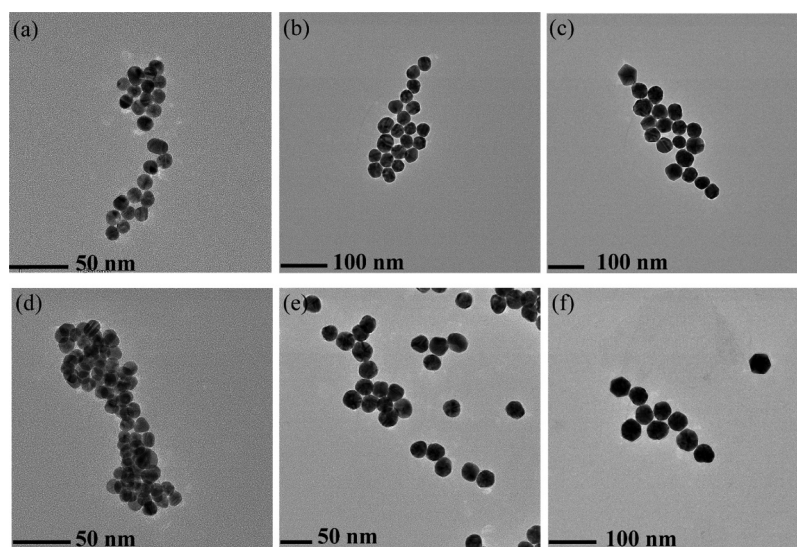
Figure 3. TEM images of PDDA−AuNPs. (a,d) 15 nm AuNPs; (b,e) 35 nm AuNPs; (c,f) 50 nm AuNPs. The concentration of repeat units PDDA was 10 μM for (a−c) and 20 μM for (d−f), respectively.

absorption wavelengths. The transient absorption spectra range from 350 to 750 nm was detected alternatively by intensified Andor iStar charge-coupled device camera. The signals from PMT were recorded by a 100 MHz oscilloscope (Tektronix, TDS 3012C). The data were analyzed and fitted by L900 software of the LP980 spectrophotometer. All the sample solutions were freshly prepared and saturated with nitrogen for each measurement.

RESULTS AND DISCUSSION

Characterization of AuNPs and PDDA−AuNPs Assembly. AuNPs with different sizes were synthesized. As shown in Figure 1a, AuNPs with distinct diameters of 15 ± 2, 35 ± 2, and 50 ± 4 nm exhibit single peak at 519, 524, and 532 nm respectively, which is in good agreement with the previous study.[46] The size of AuNPs is determined by TEM from at least five randomly selected locations. From Figure 1b, it is clearly shown that the AuNPs present spherical shape and are

separated from each other. The DLS measurements demonstrate the hydrodynamic sizes of AuNPs which agree with the results of UV−vis spectra and TEM measurements (Figure S1).

The AuNPs are negatively charged with the protection of excess citrate in the solution. PDDA, a positively charged polymer, can be utilized to assemble AuNPs, forming the aggregates through electrostatic interaction.[22] Furthermore, PDDA has no light absorption from the visible to near-IR range and thus has no interference for spectral detection.[22] The color of AuNPs solution turned purple quickly after adding PDDA, indicating AuNP aggregates have been formed.[22] As shown in Figure 2, the addition of PDDA to AuNPs solution may cause the decrease of the original SPR absorption of AuNPs at ∼530 nm, accompanying with a new spectral band centered at around 650 nm appeared in the UV−vis spectra.[47,48] According to the previous results, the longer wavelength peak at 650 nm is interpreted as arising from

longitudinal resonance absorption similar to the gold nanorods in the case of chainlike aggregation of the individual NPs. The shorter wavelength band at ~530 nm is associated with the transverse modes of the chain structures with slight red shift relative to initial single particle resonance.[7,21,22] Furthermore, TEM measurements also demonstrate that PDDA successfully assemble AuNPs-forming AuNP aggregates (Figure 3). From Figure 3, it is obvious that the degree of 15 nm AuNP aggregates assembled by PDDA is much larger than 35 and 50 nm AuNPs. The extent of AuNP aggregation can be also reflected by the UV−vis spectra, where larger aggregates have a broader aggregation plasmon peak.[49,50] As shown in Figure 2a compared with 2b,c, the 650 nm plasmon band of the aggregates is much broader which looks like an offset from the baseline because much larger aggregates are obtained for the 15 nm AuNP assembled by PDDA. Additionally, the scattering effect of AuNP aggregates assembled by PDDA could also contribute to the much broader plasmon band from 600 to 800 nm.[1] After adding PDDA into isolated AuNPs solution, the hydrodynamic sizes of AuNPs became larger and size distribution became broader. These phenomena demonstrate further the AuNP aggregate formation which is in agreement with the UV−vis spectra and TEM image (Figure S2).

To ensure the anionic dye and the commonly used photosensitizer, RB, to be adsorbed by the AuNPs aggregates, zeta potential measurements were performed and the results are listed in Table 1. Adding PDDA into the citrate-stabilized

Table 1. Zeta Potential (mV) for AuNPs, PDDA−AuNPs Assembly at Two Concentrations of PDDA (10 and 20 μM), and for AuNPs or PDDA−AuNPs after Adding RB

PDDA concentration (μM)	0	10	20
15 nm AuNPs	−28.1	3.19	6.98
15 nm AuNPs−RB	−33.5	−11.65	3.7
35 nm AuNPs	−32.7	11.05	11.85
35 nm AuNPs−RB	−34.8	1.24	7.78
50 nm AuNPs	−20.7	12.35	13.25
50 nm AuNPs−RB	−36.3	1.96	7.81

AuNPs, zeta potential changed from a negative value to a positive value. The positively charged PDDA−AuNPs assembly can thus allow for the adsorption of anionic molecules. While adding RB into the PDDA−AuNPs, zeta potential of PDDA−AuNPs decreased, which confirms that RB molecules are adsorbed to the PDDA−AuNPs because of electrostatic attraction. On the contrary, for the citrate-

stabilized AuNPs, RB molecules could not be adsorbed as indicated by the more negative zeta potential of AuNPs after the addition of RB (Table 1). This is understandable because of electrostatic repulsion between the citrate-stabilized AuNPs and the anionic dye RB.

**Triplet Excited State Enhancement by PDDA−AuNPs.** According to the ground-state UV−vis spectra (Figure 2), the PDDA−AuNPs has no enhancement effect on the absorption of the ground state of RB. After deducting the absorption intensity of PDDA−AuNPs (blue line) from that of PDDA−AuNPs−RB (green line), the absorption intensity of RB in the presence of AuNPs is obtained, which is nearly unchanged compared to that of RB alone. There is no evidence showing that the plasmon acts as an antenna to enhance the absorption.

Upon 532 nm laser irradiation, RB is pumped to the singlet excited state and further populated to the triplet excited state via ISC. The triplet state of RB was then monitored by nanosecond time-resolved UV−vis absorption spectroscopy as shown in Figure S3. In the transient spectra (Figure 4a), the negative peak at 540 nm is ascribed to the ground-state bleaching of RB. It is obvious that the triplet RB has very broad and flat T−T absorption from 380 to 750 nm in the spectra, with three resolved small peaks at 380, 465, and 590 nm. The spectral feature here agrees with the previous results.[51] Additionally, these transient features can be effectively quenched by molecular oxygen through T−T energy transfer (TTET) (Figure S4), further confirming the assignment of the triplet excited state of RB. For the 532 nm excitation of AuNPs alone, neither the isolated nor the PDDA-aggregated AuNPs display any signal in the ns transient spectra because the ultrafast photophysical processes of AuNPs have completed in ns and longer time scale.[52] This provides a neat background.

In the presence of 15 nm citrate-stabilized AuNPs, there is almost no enhancement effect on the triplet excited state of RB, as seen by the red line and black line in Figure 4a. For RB in the presence of PDDA−AuNPs assembly (the repeat unit concentration of PDDA is 20 μM), the triplet state signal of RB is greatly enhanced as can be seen from the blue line of Figure 4a at initial time delay (50 ns). The negative band of ground state bleach is superimposed on the top of the enhanced signal of the triplet state. The whole T−T absorption spectra of RB span from 380 to 750 nm, which are remarkably broad and overlap mostly with that of the ground state bleach.[51] Under the AuNPs interaction, the triplet signal of RB is enhanced in the whole spectra range during the initial several hundred nanoseconds after laser excitation. Only at long delay times (>300 ns) after the complete decay of the enhanced
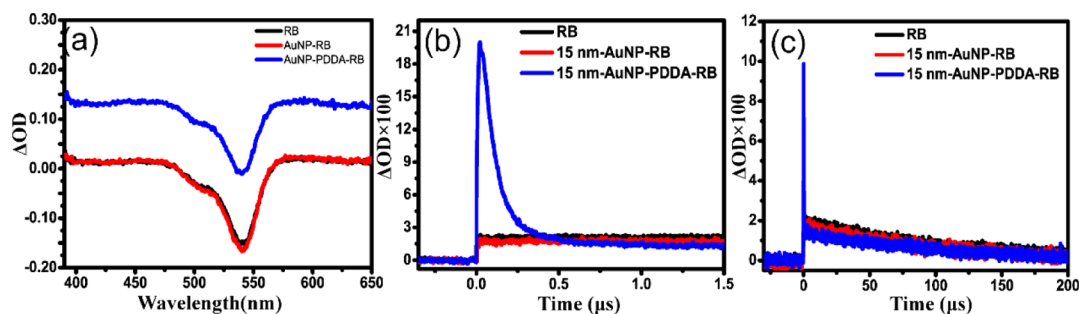
Figure 4. (a) Transient UV−vis absorption spectra of 5 μM RB (black line), RB in 15 nm AuNPs (red line) and RB in the PDDA−AuNPs (blue line), and time delay 50 ns after 532 nm laser excitation. (b,c) Decay kinetics of transient absorption at 590 nm for the triplet excited states of RB at 1.5 μs short time scale (b) and 200 μs long time scale (c).
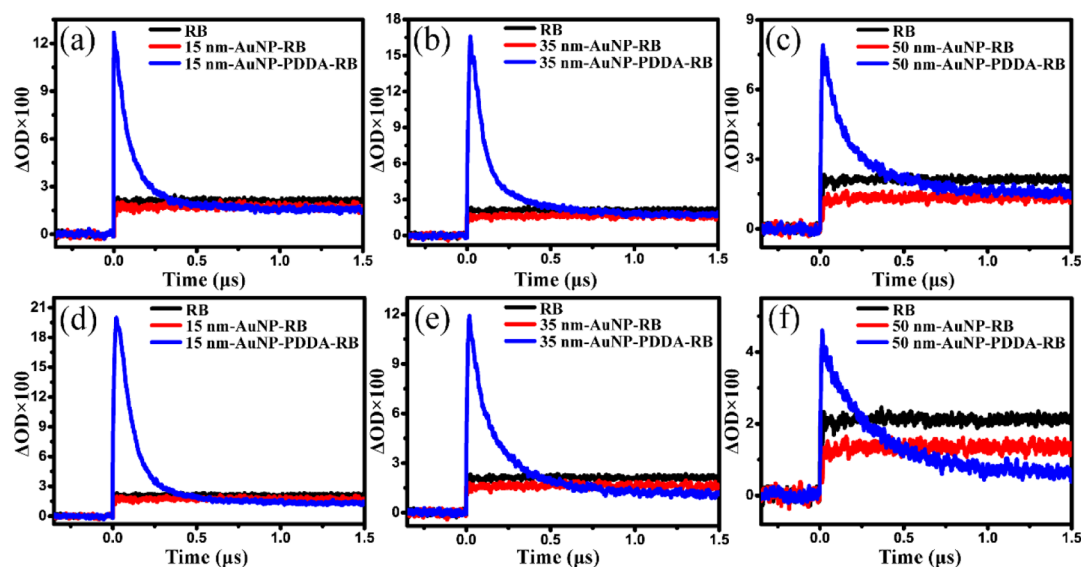
Figure 5. Triplet kinetic curves of RB adsorbed on PDDA−AuNPs. (a) RB in the 15 nm AuNP aggregates assembled by 10 μM PDDA; (b) RB in the 35 nm AuNP aggregates assembled by 10 μM PDDA; (c) RB in the 50 nm AuNP aggregates assembled 10 μM PDDA; (d) RB in the 15 nm AuNP assembled induced by 20 μM PDDA; (e) RB in the 35 nm AuNP aggregates assembled by 20 μM PDDA; (f) RB in the 50 nm AuNP aggregates assembled by 20 μM PDDA. In each graph, black lines represent the triplet decay kinetics of RB (5 μM); red lines represent the triplet decay kinetics of RB in AuNPs; blue lines represent the triplet decay kinetics of RB in the PDDA−AuNPs.

triplet signals (Figure S5), the negative peak of ground state bleach becomes clear in the transient spectra.

To quantitatively evaluate the triplet state enhancement factor, characteristic kinetics curves of the triplet peak of RB at 590 nm were measured (Figure 4b), where the triplet signal is not mixed with ground state bleach. Interestingly, in the presence of the PDDA (20 μM)−AuNPs (15 nm), the initial triplet signal intensity of the RB is significantly enhanced compared to that in the absence of AuNPs or in the presence of citrate-stabilized AuNPs, as shown in Figure 4b. The enhancement factor is ∼10-fold, which is larger than previous results (2−3 times).[27,28]

It should be noted here that because of the overlap of the ground state bleach with the triplet-state absorption of RB, the ground-state bleach kinetics alone could not be obtained. The transient signal of the negative peak at 540 nm comprises the signals of both the triplet and ground states. In the presence of PDDA−AuNPs, the ground-state bleach signal is mostly buried by the enhanced positive triplet signal, which makes the initial 300 ns kinetics of 540 nm resemble that of the 590 nm. After the decay of the enhanced triplet signal is complete (>300 ns), the kinetics of 540 nm starts to show the recovery of ground state bleach, which matches with the slow triplet decay kinetics of 590 nm (Figure S6). The slow phase (>300 ns) kinetics simply correspond to RB molecules unabsorbed and thus not interacted by AuNPs as described below.

At longer time scale of 200 μs as shown in Figure 4c, in the absence of AuNPs, the decay curve of RB can be fitted by a single exponential function and the triplet lifetime is ∼124 μs (black line). A similar temporal curve (red line) is obtained for the RB in the citrate AuNPs, meaning that the citrate AuNPs has no evident effect on the triplet state of RB. When adding RB into the PDDA (20 μM)−AuNPs (15 nm), biexponential fitting is required to illustrate the decay kinetics, which is composed of the short decay lifetime component of ∼104 ns as shown in Figure 4b and the long-time decay lifetime of ∼120 μs. The short decay component accompanied by ∼10-fold

enhancement of the triplet should correspond to the RB molecules that are truly brought into the proximity of AuNPs. The longer lifetime of ∼120 μs is similar to triplet lifetime of free RB which should then correspond to the RB molecules not in the vicinity of AuNPs.

Mechanism of the Enhancement Effect on Triplet by PDDA−AuNPs. Upon 532 nm laser excitation, the plasmon of metal NPs is excited and then affects the excited state process of nearby molecules, which can result in the enhancement of singlet excited state populations and then further populating to triplet excited state via ISC. The interparticle distance of AuNPs becomes shorter due to aggregation, which can promote the generation of higher order collective plasmonic resonance between neighboring NPs. The plasmonic resonance resulted from near field of AuNPs is inversely proportional to d^3, where d is the distance between closely spaced NPs.[53] Owing to the intense interparticle coupling, aggregated metal NPs can form extremely intense electromagnetic field called "hot-spots" which can greatly influence the excitation of adjacent molecules.[9,11,54,55]

When adding RB into the citrate AuNP, no aggregation happened because of the electrostatic repulsion between anionic RB and AuNP. In this case, AuNPs are isolated and there is no interparticle plasmon coupling. Moreover, RB cannot be adsorbed to the surface of AuNP because of electrostatic repulsion. This explains why the triplet state of RB in citrate AuNP cannot be enhanced.

In contrast, the PDDA-assembled AuNPs (15 nm) display obvious enhancement effect (∼10-fold) for the triplet signal of RB. This is probably because of the formation of dense aggregates in this case. As shown in Figures 2d and 3d, there is a strong aggregation peak at ∼650 nm and apparent dense AuNPs aggregates being observed. Hence, there should be strong interparticle coupling, and RB adsorbed in the interparticle range will be effectively modulated by strong plasmonic field, leading to triplet state enhancement. Moreover, there could be an external heavy atom effect of Au

particle affecting RB molecules in proximity. However, if the heavy atom effect dominates the triplet enhancement but not the plasmonic effects, the enhancement factor should have no relationship with the extent of AuNP aggregation assembled by PDDA. According to our experiment results, the triplet enhancement factor is quite sensitive to the extent of AuNP aggregation assembled by PDDA. Therefore, the plasmon effect mainly contributes to the triplet state enhancement and the heavy atom effect should be minor.

In principle, the plasmonic effect of AuNPs can accelerate the ISC from S_1 to T_1, resulting in the enhanced triplet formation yield.[37] Although the enhanced S_1 to T_1 rate could not be observed in the ns time range, we see the accelerated ISC process of T_1 to S_0, as manifested by the dramatically shortened decay component (∼104 ns) accompanied with ∼10-fold triplet signal enhancement. This gives clear evidence for the acceleration of ISC by AuNP plasmon. Meanwhile, the enhancement of the cross section for T−T absorption cross section may also contribute to the enhanced triplet signal.

Interestingly, when the different size of AuNPs was assembled by PDDA, a different enhancement effect was observed (Figure 5). When using PDDA (repeat unit concentration of 20 μM) to assemble AuNPs of 15, 35 and 50 nm, as shown in Figure 5d−f, there is a decreased enhancement factor of the triplet state from 15 nm (10 fold), to 35 nm (6 fold), and 50 nm (2.4 fold).

This seems to be related to the capability of PDDA in assembling different sizes of AuNPs. As shown in Figures 2e,f and 3e,f, as the size of AuNPs increases from 15 nm, to 35 nm, and 50 nm, the AuNP aggregation peak intensity at ∼650 nm decreases and TEM shows a loose structure of AuNPs aggregates. Therefore, less interparticle coupling is formed for larger AuNPs assembled by PDDA and there is less enhancement effect.

Meanwhile, the overall enhancement effect on the triplet state of RB is the balance of enhancement and quenching by the adjacent AuNPs.[26,28] The increased formation of the triplet excited state of RB can be observed just in the situation when the enhancement effect is stronger than the quenching effect. The larger quenching effect for larger AuNPs should be another factor that renders the less enhancement triplet effect from larger AuNPs assembled by PDDA. As shown in Figure 5, the triplet signal of RB in the presence of AuNPs is slightly weaker than that of RB itself, meaning less formation of triplet RB initially. This quenching is more obvious for the larger size of AuNPs (50 nm) and does not affect the decay dynamics, indicating it is some sort of static effect, most likely, because of the shielding of RB molecules by the large 50 nm AuNPs which reduces the number of molecules excited by the laser and probed by the xenon lamp. Therefore, to obtain higher enhancement factors on the triplet excited state, it is necessary to consider the appropriate NP size and its surface property.

Additionally, the influence of PDDA concentration is also considered. On adding 5 μM PDDA in 15 nm AuNPs solution, the zeta potential of PDDA−AuNPs still displays a negative value. The anionic RB could not be effectively adsorbed in the vicinity of AuNPs because of electrostatic repulsion, and there is no triplet state enhancement by AuNPs being observed. The triplet state enhance factor could reach 6.5- and 10-fold after the addition of 10 and 20 μM PDDA into the 15 nm AuNPs solution, respectively, as shown in Figure 5a,d. For the small size of AuNPs, larger concentration of PDDA is more suitable to assemble AuNPs forming aggregates. As shown in Figure 2d,

there is a stronger aggregation peak at 650 nm and denser aggregate structure observed for 20 μM PDDA-assembled AuNPs (15 nm). For the larger size of AuNPs (35 or 50 nm), it appears that smaller concentration of PDDA (10 μM) is favorable for the formation of AuNPs aggregates, as shown by the stronger peak at 650 nm in Figure 2b,c compared to 2e,f. This can also be seen by the TEM image in Figure 3b,c compared to 3e,f. These results explain the decrease of the triplet state enhancement factor from 8.5- to 6-fold after the addition of 10 and 20 μM PDDA into 35 nm AuNPs solution (Figure 5b,e).

In general, both the AuNPs size and the PDDA concentration can affect the degree of aggregation, while the degree of AuNP aggregation is closely related to the triplet enhancement factors. The polymer has both the effects of flocculation that promotes aggregation and steric stability that prevents aggregation. For the smaller particle size of 15 nm AuNPs with a larger surface area, larger concentration PDDA to neutralize surface charge of AuNPs are favorable for the formation of higher degree of AuNP aggregates. For the larger size AuNPs with a smaller surface area, smaller concentration of PDDA is needed to neutralize surface charge of AuNPs. Further addition of PDDA then has the steric stability effect that prevents aggregation. Therefore, higher concentration of PDDA is not beneficial for the formation of aggregates for the larger size of AuNPs. These observations provide insights for guiding the practical regulation of NP aggregation by the polymer, which is a useful strategy enhancing the AuNPs plasmon effect.

As indicated above, the formation of AuNP aggregates upon the addition of a positively charged polymer PDDA is the most important factor for the enhancement of the triplet state of dye molecules adjacent to the AuNPs. The PDDA can well regulate the formation of aggregates such that a higher enhancement effect of AuNP plasmon has been achieved. This is in contrast to previous results,[27,28] where only 2−3 times of the triplet state enhancement effect was displayed for the cationic dye molecules (methylene blue) adsorbed by the citrate coated AuNPs. Obviously, the simple increasing of the dye molecule interaction with the AuNPs due to a change in surface charge cannot have a large enhancement effect. Our findings point to the possibilities of using polymer assembled AuNPs to enhance the triplet state formation, which is the key transient governing many spectroscopic and energy transformation processes.

■ CONCLUSIONS

In this work, water soluble cationic polymer PDDA is applied to assemble the AuNPs forming aggregates (PDDA−AuNPs). After adding PDDA, the zeta potential of PDDA−AuNPs is obviously changed, indicating the adsorption of anionic dye molecule RB onto AuNPs through electrostatic attraction. The triplet formation of RB upon 532 nm pulsed laser excitation was directly monitored by means of time-resolved UV−visible absorption spectroscopy. Maximum ∼10 fold enhancement effect on the triplet formation of RB is obtained. The large enhancement should be resulted from the PDDA−AuNPs aggregation mainly through the plasmon effect. Additionally, it is found that the triplet state enhancement effect of PDDA-assembled AuNPs is sensitive to the concentration of the polymer and the size of AuNPs. As the size of AuNPs increases from 15 nm, to 35 nm, and 50 nm, there is a decreased enhancement effect because the larger size AuNPs are less densely assembled by PDDA and there are less interparticle

coupling. Meanwhile, for the small size of AuNPs, larger concentration of PDDA is more suitable to assemble AuNPs forming aggregates and thus displays a larger enhancement effect. These findings reveal the strong interaction of plasmon affecting the triplet excited state population dynamics. Plenty of new applications can thus be enabled using the polymer-assembled AuNP aggregates on TTET, triplet exciton harvesting and photodynamic therapy, and so forth.

■ ASSOCIATED CONTENT

Ⓢ Supporting Information

The Supporting Information is available free of charge on the ACS Publications website at DOI: 10.1021/acs.jpcc.9b06094.

Corresponding figures for DLS measurement of AuNPs; decay kinetics of transient absorption at 590 nm for RB under N_2-saturated and air-saturated conditions; transient UV−vis absorption spectrum of RB in the presence of PDDA−AuNPs; and decay kinetics of transient absorption at 540 and 590 nm for RB in the absence and presence of PDDA−AuNPs (PDF)

■ AUTHOR INFORMATION

Corresponding Authors

*E-mail: kunhui@bnu.edu.cn (K.L.).
*E-mail: hongmei@bnu.edu.cn (H.S.).

ORCID Ⓞ

Hongmei Su: 0000-0001-7384-6523

Notes

The authors declare no competing financial interest.

■ ACKNOWLEDGMENTS

■ REFERENCES

(1) Li, M.; Cushing, S. K.; Wu, N. Plasmon-Enhanced Optical Sensors: A Review. *Analyst* **2015**, *140*, 386−406.

(2) Barazzouk, S.; Kamat, P. V.; Hotchandani, S. Photoinduced Electron Transfer between Chlorophyll A and Gold Nanoparticles. *J. Phys. Chem. B* **2005**, *109*, 716−723.

(3) Murphy, S.; Huang, L.; Kamat, P. V. Charge-Transfer Complexation and Excited-State Interactions in Porphyrin-Silver Nanoparticle Hybrid Structures. *J. Phys. Chem. C* **2011**, *115*, 22761−22769.

(4) Adams, M.; Kozlowska, M.; Baroni, N.; Oldenburg, M.; Ma, R.; Busko, D.; Turshatov, A.; Emandi, G.; Senge, M. O.; Haldar, R.; et al. Highly Efficient One-Dimensional Triplet Exciton Transport in a Palladium−Porphyrin-Based Surface-Anchored Metal−Organic Framework. *ACS Appl. Mater. Interfaces* **2019**, *11*, 15688−15697.

(5) Planas, O.; Macia, N.; Agut, M.; Nonell, S.; Heyne, B. Distance-Dependent Plasmon-Enhanced Singlet Oxygen Production and Emission for Bacterial Inactivation. *J. Am. Chem. Soc.* **2016**, *138*, 2762−2768.

(6) Giannini, V.; Fernández-Domínguez, A. I.; Heck, S. C.; Maier, S. A. Plasmonic Nanoantennas: Fundamentals and Their Use in Controlling the Radiative Properties of Nanoemitters. *Chem. Rev.* **2011**, *111*, 3888−3912.

(7) Polavarapu, L.; Xu, Q.-H. Water-Soluble Conjugated Polymer-Induced Self-Assembly of Gold Nanoparticles and Its Application to SERS. *Langmuir* **2008**, *24*, 10608−10611.

(8) Li, J. F.; Huang, Y. F.; Ding, Y.; Yang, Z. L.; Li, S. B.; Zhou, X. S.; Fan, F. R.; Zhang, W.; Zhou, Z. Y.; Wu, D. Y.; et al. Shell-Isolated

Nanoparticle-Enhanced Raman Spectroscopy. *Nature* **2010**, *464*, 392−395.

(9) Qian, K.; Liu, H.; Yang, L.; Liu, J. Designing and Fabricating of Surface-Enhanced Raman Scattering Substrate with High Density Hot Spots by Polyaniline Template-Assisted Self-Assembly. *Nanoscale* **2012**, *4*, 6449−6454.

(10) Wei, L.; Jin, B.; Dai, S. Polymer Microbead-Based Surface Enhanced Raman Scattering Immunoassays. *J. Phys. Chem. C* **2012**, *116*, 17174−17181.

(11) Liu, H.; Yang, Z.; Meng, L.; Sun, Y.; Wang, J.; Yang, L.; Liu, J.; Tian, Z. Three-Dimensional and Time-Ordered Surface-Enhanced Raman Scattering Hotspot Matrix. *J. Am. Chem. Soc.* **2014**, *136*, 5332−5341.

(12) Ding, S.-Y.; You, E.-M.; Tian, Z.-Q.; Moskovits, M. Electromagnetic Theories of Surface-Enhanced Raman Spectroscopy. *Chem. Soc. Rev.* **2017**, *46*, 4042−4076.

(13) Li, J.-F.; Zhang, Y.-J.; Ding, S.-Y.; Panneerselvam, R.; Tian, Z.-Q. Core-Shell Nanoparticle-Enhanced Raman Spectroscopy. *Chem. Rev.* **2017**, *117*, 5002−5069.

(14) Anger, P.; Bharadwaj, P.; Novotny, L. Enhancement and Quenching of Single-Molecule Fluorescence. *Phys. Rev. Lett.* **2006**, *96*, 113002.

(15) Kinkhabwala, A.; Yu, Z.; Fan, S.; Avlasevich, Y.; Müllen, K.; Moerner, W. E. Large Single-Molecule Fluorescence Enhancements Produced by a Bowtie Nanoantenna. *Nat. Photonics* **2009**, *3*, 654−657.

(16) Guerrero, A. R.; Aroca, R. F. Surface-Enhanced Fluorescence with Shell-Isolated Nanoparticles (SHINEF). *Angew. Chem., Int. Ed.* **2011**, *50*, 665−668.

(17) Gill, R.; Tian, L.; Somerville, W. R. C.; Le Ru, E. C.; van Amerongen, H.; Subramaniam, V. Silver Nanoparticle Aggregates as Highly Efficient Plasmonic Antennas for Fluorescence Enhancement. *J. Phys. Chem. C* **2012**, *116*, 16687−16693.

(18) Geddes, C. D.; Cao, H.; Gryczynski, I.; Gryczynski, Z.; Fang, J.; Lakowicz, J. R. Metal-Enhanced Fluorescence (MEF) Due to Silver Colloids on a Planar Surface: Potential Applications of Indocyanine Green to in Vivo Imaging. *J. Phys. Chem. A* **2003**, *107*, 3443−3449.

(19) Shen, S.; Meng, L.; Zhang, Y.; Han, J.; Ma, Z.; Hu, S.; He, Y.; Li, J.; Ren, B.; Shih, T.-M.; et al. Plasmon-Enhanced Second-Harmonic Generation Nanorulers with Ultrahigh Sensitivities. *Nano Lett.* **2015**, *15*, 6716−6721.

(20) Davidson, R. B.; Yanchenko, A.; Ziegler, J. I.; Avanesyan, S. M.; Lawrie, B. J.; Haglund, R. F. Ultrafast Plasmonic Control of Second Harmonic Generation. *ACS Photonics* **2016**, *3*, 1477−1481.

(21) Guan, Z.; Polavarapu, L.; Xu, Q.-H. Enhanced Two-Photon Emission in Coupled Metal Nanoparticles Induced by Conjugated Polymers. *Langmuir* **2010**, *26*, 18020−18023.

(22) Han, F.; Guan, Z.; Tan, T. S.; Xu, Q.-H. Size-Dependent Two-Photon Excitation Photoluminescence Enhancement in Coupled Noble-Metal Nanoparticles. *ACS Appl. Mater. Interfaces* **2012**, *4*, 4746−4751.

(23) Guan, Z.; Gao, N.; Jiang, X.-F.; Yuan, P.; Han, F.; Xu, Q.-H. Huge Enhancement in Two-Photon Photoluminescence of Au Nanoparticle Clusters Revealed by Single-Particle Spectroscopy. *J. Am. Chem. Soc.* **2013**, *135*, 7272−7277.

(24) Jiang, X.-F.; Pan, Y.; Jiang, C.; Zhao, T.; Yuan, P.; Venkatesan, T.; Xu, Q.-H. Excitation Nature of Two-Photon Photoluminescence of Gold Nanorods and Coupled Gold Nanoparticles Studied by Two-Pulse Emission Modulation Spectroscopy. *J. Phys. Chem. Lett.* **2013**, *4*, 1634−1638.

(25) Zhang, Y.; Aslan, K.; Malyn, S. N.; Geddes, C. D. Metal-Enhanced Phosphorescence (MEP). *Chem. Phys. Lett.* **2006**, *427*, 432−437.

(26) Meng, M.; Zhang, F.-L.; Yi, J.; Lin, L.-H.; Zhang, C.-L.; Bodappa, N.; Li, C.-Y.; Zhang, S.-J.; Aroca, R. F.; Tian, Z.-Q.; et al. Shell-Isolated Nanoparticle-Enhanced Phosphorescence. *Anal. Chem.* **2018**, *90*, 10837−10842.

(27) Pacioni, N. L.; González-Béjar, M.; Alarcón, E.; McGilvray, K. L.; Scaiano, J. C. Surface Plasmons Control the Dynamics of Excited

Triplet States in the Presence of Gold Nanoparticles. *J. Am. Chem. Soc.* **2010**, *132*, 6298−6299.

(28) Yang, W.; Liu, K.; Song, D.; Du, Q.; Wang, R.; Su, H. Aggregation-Induced Enhancement Effect of Gold Nanoparticles on Triplet Excited State. *J. Phys. Chem. C* **2013**, *117*, 27088−27095.

(29) Glotzer, S. C.; Horsch, M. A.; Iacovella, C. R.; Zhang, Z.; Chan, E. R.; Zhang, X. Self-Assembly of Anisotropic Tethered Nanoparticle Shape Amphiphiles. *Curr. Opin. Colloid Interface Sci.* **2005**, *10*, 287−295.

(30) Liu, K.; Zhao, N.; Kumacheva, E. Self-Assembly of Inorganic Nanorods. *Chem. Soc. Rev.* **2011**, *40*, 656−671.

(31) Shibu Joseph, S. T.; Ipe, B. I.; Pramod, P.; Thomas, K. G. Gold Nanorods to Nanochains: Mechanistic Investigations on Their Longitudinal Assembly Using *α,ω*-Alkanedithiols and Interplasmon Coupling. *J. Phys. Chem. B* **2006**, *110*, 150−157.

(32) Pramod, P.; Thomas, K. G. Plasmon Coupling in Dimers of Au Nanorods. *Adv. Mater.* **2008**, *20*, 4300−4305.

(33) Lee, J. H.; Wernette, D. P.; Yigit, M. V.; Liu, J.; Wang, Z.; Lu, Y. Site-Specific Control of Distances Between Gold Nanoparticles Using Phosphorothioate Anchors on DNA and a Short Bifunctional Molecular Fastener. *Angew. Chem., Int. Ed.* **2007**, *46*, 9006−9010.

(34) Chen, Z.; Tan, Y.; Zhang, C.; Yin, L.; Ma, H.; Ye, N.; Qiang, H.; Lin, Y. A Colorimetric Aptamer Biosensor Based on Cationic Polymer and Gold Nanoparticles for the Ultrasensitive Detection of Thrombin. *Biosens. Bioelectron.* **2014**, *56*, 46−50.

(35) Xi, H.; He, W.; Liu, Q.; Chen, Z. Protein Discrimination Using a Colorimetric Sensor Array Based on Gold Nanoparticle Aggregation Induced by Cationic Polymer. *ACS Sustainable Chem. Eng.* **2018**, *6*, 10751−10757.

(36) Jin, S.; Sugawa, K.; Takeshima, N.; Tahara, H.; Igari, S.; Yoshinari, S.; Kurihara, Y.; Watanabe, S.; Enoki, M.; Sato, K.; et al. Precise Control of Localized Surface Plasmon Wavelengths Is Needed for Effective Enhancement of Triplet−Triplet Annihilation-Based Upconversion Emission. *ACS Photonics* **2018**, *5*, 5025−5037.

(37) Cao, X.; Hu, B.; Ding, R.; Zhang, P. Plasmon-Enhanced Homogeneous and Heterogeneous Triplet-Triplet Annihilation by Gold Nanoparticles. *Phys. Chem. Chem. Phys.* **2015**, *17*, 14479−14483.

(38) Qu, Z.; Duan, P.; Zhou, J.; Wang, Y.; Liu, M. Photon Upconversion in Organic Nanoparticles and Subsequent Amplification by Plasmonic Silver Nanowires. *Nanoscale* **2018**, *10*, 985−991.

(39) Bujak, Ł.; Narushima, K.; Sharma, D. K.; Hirata, S.; Vacha, M. Plasmon Enhancement of Triplet Exciton Diffusion Revealed by Nanoscale Imaging of Photochemical Fluorescence Upconversion. *J. Phys. Chem. C* **2017**, *121*, 25479−25486.

(40) Khaing Oo, M. K.; Yang, Y.; Hu, Y.; Gomez, M.; Du, H.; Wang, H. Gold Nanoparticle-Enhanced and Size-Dependent Generation of Reactive Oxygen Species from Protoporphyrin IX. *ACS Nano* **2012**, *6*, 1939−1947.

(41) Lucky, S. S.; Soo, K. C.; Zhang, Y. Nanoparticles in Photodynamic Therapy. *Chem. Rev.* **2015**, *115*, 1990−2042.

(42) Frens, G. Controlled Nucleation for the Regulation of the Particle Size in Monodisperse Gold Suspensions. *Nat. Phys. Sci.* **1973**, *241*, 20−22.

(43) Enustun, B. V.; Turkevich, J. Coagulation of Colloidal Gold. *J. Am. Chem. Soc.* **1963**, *85*, 3317−3328.

(44) Bastús, N. G.; Comenge, J.; Puntes, V. Kinetically Controlled Seeded Growth Synthesis of Citrate-Stabilized Gold Nanoparticles of up to 200 nm: Size Focusing versus Ostwald Ripening. *Langmuir* **2011**, *27*, 11098−11105.

(45) Wu, L.; Liu, K.; Jie, J.; Song, D.; Su, H. Direct Observation of Guanine Radical Cation Deprotonation in G-quadruplex DNA. *J. Am. Chem. Soc.* **2015**, *137*, 259−266.

(46) Haiss, W.; Thanh, N. T. K.; Aveyard, J.; Fernig, D. G. Determination of Size and Concentration of Gold Nanoparticles from UV−Vis Spectra. *Anal. Chem.* **2007**, *79*, 4215−4221.

(47) Weisbecker, C. S.; Merritt, M. V.; Whitesides, G. M. Molecular Self-Assembly of Aliphatic Thiols on Gold Colloids. *Langmuir* **1996**, *12*, 3763−3772.

(48) Kamat, P. V.; Barazzouk, S.; Hotchandani, S. Electrochemical Modulation of Fluorophore Emission on a Nanostructured Gold Film. *Angew. Chem., Int. Ed.* **2002**, *41*, 2764−2767.

(49) Alba-Molina, D.; Martín-Romero, M.; Camacho, L.; Giner-Casares, J. Ion-Mediated Aggregation of Gold Nanoparticles for Light-Induced Heating. *Appl. Sci.* **2017**, *7*, 916.

(50) Ghosh, S. K.; Pal, T. Interparticle Coupling Effect on the Surface Plasmon Resonance of Gold Nanoparticles: From Theory to Applications. *Chem. Rev.* **2007**, *107*, 4797−4862.

(51) Ludvíková, L.; Friš, P.; Heger, D.; Šebej, P.; Wirz, J.; Klán, P. Photochemistry of Rose Bengal in Water and Acetonitrile: A Comprehensive Kinetic Analysis. *Phys. Chem. Chem. Phys.* **2016**, *18*, 16266−16273.

(52) Jain, P. K.; Qian, W.; El-Sayed, M. A. Ultrafast Electron Relaxation Dynamics in Coupled Metal Nanoparticles in Aggregates. *J. Phys. Chem. B* **2006**, *110*, 136−142.

(53) Chang, W.-S.; Willingham, B.; Slaughter, L. S.; Dominguez-Medina, S.; Swanglap, P.; Link, S. Radiative and Nonradiative Properties of Single Plasmonic Nanoparticles and Their Assemblies. *Acc. Chem. Res.* **2012**, *45*, 1936−1945.

(54) Zhou, X.; Zhou, F.; Liu, H.; Yang, L.; Liu, J. Assembly of Polymer-Gold Nanostructures with High Reproducibility into a Monolayer Film SERS Substrate with 5 nm Gaps for Pesticide Trace Detection. *Analyst* **2013**, *138*, 5832−5838.

(55) Nah, S.; Li, L.; Fourkas, J. T. Field-Enhanced Phenomena of Gold Nanoparticles. *J. Phys. Chem. A* **2009**, *113*, 4416−4422.